Journal of The Electrochemical Society, **153** (6) A1193-A1200 (2006)
0013-4651/2006/153(6)/A1193/8/$20.00 © The Electrochemical Society

A Nonisothermal, Two-Phase Model for Polymer Electrolyte Fuel Cells

Yun Wang* **and Chao-Yang Wang****,z**

Electrochemical Engine Center and Department of Mechanical and Nuclear Engineering, The Pennsylvania State University, University Park, Pennsylvania 16802, USA

A model fully coupling the two-phase flow, species transport, heat transfer, and electrochemical processes is developed to investigate liquid water distribution and flooding in polymer electrolyte fuel cells (PEFCs) under nonisothermal conditions. The thermal model accounts for irreversible heat and entropic heat generated due to electrochemical reactions, Joule heating arising from protonic/electronic resistance, and latent heat of water condensation and/or evaporation. A theoretical analysis is presented to show that in the two-phase zone, water transport via vapor-phase diffusion under the temperature gradient is not negligible, with a magnitude comparable to the water production rate in PEFCs. Detailed numerical results further reveal that the vapor-phase diffusion enhances water removal from the gas diffusion layer (GDL) under the channel and exacerbates GDL flooding under the land. Simultaneously, this vapor-phase diffusion provides a new mechanism for heat removal through a phase change process in which water evaporates at the hotter catalyst layer, diffuses through the interstitial spaces of the GDL, and condenses on the cooler land surface. This new heat removal mechanism resembles the heat pipe effect. Three-dimensional simulations for a full PEFC using this nonisothermal, two-phase model are presented for the first time. Separate velocity fields of gas and liquid phases are given, clearly illustrating that the vapor-phase diffusion and capillary-driven liquid water transport in a GDL aid each other in water removal along the through-plane direction under the channel area, but oppose each other along the in-plane direction between the channel area and land.
 [DOI: 10.1149/1.2193403]

Manuscript submitted October 17, 2005; revised manuscript received February 20, 2006. Available electronically April 26, 2006.

One of the most complex and vital phenomena in polymer electrolyte fuel cells (PEFCs) is two-phase transport, originating from water production by the oxygen reduction reaction in the cathode.[1] Liquid droplets may block pore paths of mass transport through porous diffusion media and catalyst layers, thereby reducing PEFC performance and further leading to cell degradation.[2,3] Because the formation of liquid water depends on the water vapor saturation pressure, which is a strong function of temperature, the temperature field and its coupling with water condensation and/or evaporation are critical to the study of two-phase transport and the ensuing cathode flooding in a PEFC.

Mathematical modeling of heat transfer[4-7] and two-phase transport[8-18] in PEFCs has been carried out by several groups. Unfortunately, the majority of past research has dealt with only one aspect, either a two-phase model under isothermal conditions or a nonisothermal model under single-phase (dry) conditions. The incorporation of both phenomena has been attempted by Nam and Kaviany[19] and Rowe and Li,[20] both of which are one-dimensional. The model of Nam and Kaviany[19] focused on two-phase flow through the cathode GDL and explored the influences of fiber diameter, porosity, and capillary pressure on the liquid water removal rate. Rowe and Li's[20] model is more comprehensive, involving the multicomponent transport of hydrogen, oxygen, and liquid water/vapor, as well as the transport of protons in the electrolyte and electrons in the electronic phase.

Most recently, Yuan and Sunden[21] presented a nonisothermal, two-phase model in multidimensional situations. However, only the cathode GDL and gas channel were considered. Costamagna[22] also developed a multi-D model in which phase change heat transfer was ignored. Berning and Djlali[23] presented a two-phase model considering heat release/absorption due to phase change. This two-phase model adopted the unsaturated flow theory (UFT) for two-phase flow through porous media,[24] which assumes a constant gas-phase pressure across the porous medium. A recent study has been performed to compare UFT with two-fluid models or the multiphase mixture model (M^2 model).[16] Another major assumption of Berning and Djlali's model is the catalyst layer as an interface without thickness. The same assumption was also involved in the work of Dutta et al.,[25,26] which is, in addition, a single-phase model. The work of Mazumder and Cole[27] was based on the M^2 model of Wang and Cheng[24] and developed for hydrophilic GDLs. There was no explicit description of water transport through the membrane in Mazumder and Cole's model. In contrast to the M^2 approach, Birgersson et al.[28] recently presented a nonisothermal separate flow model, consisting of separate equations to describe water transport in liquid and gas phases, respectively. However, they ignored entropic heat and irreversible heat generation from electrochemical reactions, and also treated the catalyst layer as an interface, thus failing to accurately address the coupling between two-phase and thermal transport processes in PEFCs. In addition, only heat and charge equations are solved in the anode, while the transport of hydrogen and water in the anode binary mixture are ignored.

The objective of the present work is to expand upon the M^2 model of Wang and co-workers[8,16,17] by incorporating the nonisothermal effect and hence addressing the intricate interactions between the two-phase flow and thermal transport. The thermal model accounts rigorously for the heat generation sources in a PEFC, i.e., irreversible heat and entropic heat generated from electrochemical reactions, Joule heating arising from protonic/electronic resistance, and phase change latent heat. In addition, a detailed membrane-electrode assembly (MEA) model is used to describe the cotransport of water and protons in the membrane and electrodes. Numerical simulations for a single-channel PEFC, along with a theoretical analysis, are performed.

Physical and Numerical Model

A steady-state model of PEFCs consists of five principles of conservation: mass, momentum, energy, species, and charge. These can be presented in concise form as follows[16,29,30]

Continuity equation $$\nabla\cdot(\rho\vec{u}) = 0 \quad [1]$$

Momentum conservation $$\frac{1}{\epsilon^2}\nabla\cdot(\rho\vec{u}\vec{u}) = -\nabla P + \nabla\cdot\rho\tau + S_u \quad [2]$$

Energy conservation $$\nabla\cdot(\gamma_T\rho c_p\vec{u}T) = \nabla\cdot(k^{\text{eff}}\nabla T) + S_T \quad [3]$$

Species conservation

$$\nabla\cdot(\gamma_c\vec{u}C^k) = \nabla\cdot(D_g^{k,\text{eff}}\nabla C_g^k) - \nabla\cdot\left[\left(\frac{mf_l^k}{M^k} - \frac{C_g^k}{\rho_g}\right)\vec{j}_l\right] + S_k \quad [4]$$

* Electrochemical Society Student Member.
** Electrochemical Society Active Member.
z E-mail: cxw31@psu.edu

Table I. Physical and transport properties.

Quantity	Value
Water saturation concentration,[36] $C_{\text{sat}}(T)$	$C_{\text{sat}}(T) = \dfrac{P^{\text{sat}}(T)}{RT}$, where
	$\log_{10} p^{\text{sat}} = -2.1794 + 0.02953(T - 273.15) - 9.1837 \times 10^{-5}(T - 273.15)^2 + 1.4454 \times 10^{-7}(T - 273.15)^3$
Water content in membrane,[36] λ	$\lambda = \begin{cases} 0.043 + 17.81a - 39.85a^2 + 36.0a^3 & \text{for } 0 < a \leqslant 1 \\ 14 + 1.4(a - 1) & \text{for } 1 \leqslant a \leqslant 3 \end{cases}$
Ionic conductivity of membrane,[36] κ	$(0.005139\lambda - 0.00326)\exp\left[1268\left(\dfrac{1}{303} - \dfrac{1}{T}\right)\right]$
H_2O diffusivity in membrane,[37] D_{w}^{m}	$D_{\text{w}}^{m} = \begin{cases} 3.1 \times 10^{-3}\lambda(e^{0.28\lambda} - 1) \cdot e^{[-2436/T]} & \text{for } 0 < \lambda \leqslant 3 \\ 4.17 \times 10^{-4}\lambda(1 + 161e^{-\lambda}) \cdot e^{[-2436/T]} & \text{otherwise} \end{cases}$
Electro-osmotic coefficient,[38] n_d	$n_d = \begin{cases} 1.0 \text{ for } \lambda \leqslant 14 \\ \dfrac{1.5}{8}(\lambda - 14) + 1.0 \text{ otherwise} \end{cases}$
Membrane density,[39] ρ	$\rho = \dfrac{1.98 + 0.0324\lambda}{1 + 0.0648\lambda} \times 10^3$
Diffusivity in the gas channels,[40] D	$D_o\left(\dfrac{T}{353}\right)^{3/2}\left(\dfrac{1}{p}\right)$
H_2/H_2O diffusivity in anode gas at standard condition,[41] $D_{o,\text{H}_2,\text{a}}/D_{o,\text{w,a}}$	$1.1028 \times 10^{-4}/1.1028 \times 10^{-4}$ m^2/s
O_2/H_2O diffusivity in cathode gas at standard condition,[41] $D_{o,\text{O}_2,\text{c}}/D_{o,\text{w,c}}$	$3.2348 \times 10^{-5}/3.89 \times 10^{-5}$ m^2/s
Viscosity of anode/cathode gas,[42] μ	$\mu = 9.88 \times 10^{-6}X_{\text{H}_2} + 1.12 \times 10^{-5}X_{\text{H}_2\text{O}} + 2.01 \times 10^{-5}X_{\text{N}_2} + 2.3 \times 10^{-5}X_{\text{O}_2}$

Charge conservation (electrons) $0 = \nabla\cdot(\sigma^{\text{eff}}\nabla\Phi_s) + S_{\phi_s}$ [5]

Charge conservation (protons) $0 = \nabla\cdot(\kappa^{\text{eff}}\nabla\Phi_e) + S_{\phi_e}$ [6]

where ρ, $\vec{u}$, p, T, C^k, Φ_s, and Φ_e, respectively, denote the density, superficial fluid velocity vector, pressure, temperature, molar concentration of species k, electronic phase potential, and electrolyte phase potential. The assumptions made in the present model are as follows: (*i*) ideal gas mixtures; (*ii*) isotropic and homogeneous membrane, catalyst layers, and gas diffusion layers; (*iii*) incompressible and laminar flow due to small pressure gradients and flow velocity; and (*iv*) negligible mass source/sink in the continuity equation as justified in Ref. 31. The physical, transport, and electrochemical properties as well as the source terms, S_u, S_k, S_{ϕ_e}, and S_{ϕ_s}, are summarized in Tables I-III in detail. Discussion of these property relations has been presented previously and is therefore not repeated here. Other properties related to two-phase phenomena and thermal transport, i.e., the two main features of the present work, are elaborated below.

Two-phase transport.— The two-phase mixture density is defined as[16,17,24]

$$\rho = s\rho_l + (1 - s)\rho_g \quad [7]$$

where the liquid water saturation, s, is the volume fraction of open pores occupied by liquid water. In the M^2 model, the liquid saturation is obtained from the following relation with the mixture water concentration, $C^{\text{H}_2\text{O}}$, after the latter is solved from the differential equation 4

$$s = \frac{C^{\text{H}_2\text{O}} - C_{\text{sat}}}{\rho_l/M^{\text{H}_2\text{O}} - C_{\text{sat}}} \quad [8]$$

The flow fields of both phases in the GDL are described through the relative permeability, k_{rl} and k_{rg}, defined as the ratio of the intrinsic permeability of liquid and gas phases, respectively, to the total intrinsic permeability of a porous medium. Physically, these parameters describe the extent to which one fluid is hindered by others in pore spaces, and hence can be formulated as a function of

Table II. Source terms for the conservation equations in each region.[29,41]

	S_u	S_k	S_{ϕ_e}	S'_{ϕ_e}
Gas channels	0	0	-	0
Diffusion layers	$-\dfrac{\mu}{K_{\text{GDL}}}\vec{u}$	0	0	0
Catalyst layer	$-\dfrac{\mu}{K_{\text{CL}}}\vec{u}$	$-\nabla\cdot\left(\dfrac{n_d}{F}i_e\right) - \frac{s_k j}{n_k F}$	j	$-j$
Membrane	-	0	0	-
Electrochemical reaction $\Sigma s_k M_k^z = ne^-$		where	$M_k \equiv$ chemical formula of species k $s_k \equiv$ stoichiometry coefficient $n \equiv$ number of electrons transferred	
In PEM fuel cells, there are (Anode) $H_2 - 2H^+ = 2e^-$ (Cathode) $2H_2O - O_2 - 4H^+ = 4e^-$				

Note: n_d is the electro-osmotic drag coefficient for water. For H_2 and O_2, $n_d = 0$.

Table III. Electrochemical properties.[29,41]

Description	Anode	Cathode
Transfer current density, j(A/m^3)	$ai_{0,a}\left(\frac{C_{H_2}}{C_{H_2,ref}}\right)^{1/2}\left(\frac{\alpha_a+\alpha_c}{RT}\cdot F\cdot\eta\right)$	$-ai_{0,c}\exp\left[-16456\left(\frac{1}{T}-\frac{1}{353.15}\right)\right]\left(\frac{C_{O_2}}{C_{O_2,ref}}\right)\exp\left(-\frac{\alpha_c F}{RT}\cdot\eta\right)$
Surface overpotential, η (V)	$\Phi_s-\Phi_e-U_o$	$\Phi_s-\Phi_e-U_o$
Equilibrium potential, U_o (V)	0	$1.23-0.9\times10^{-3}(T-298)$
Exchange current density x reaction surface area, a_0i_0 (A/m^3)	1.0×10^9	10^4
Transfer coefficient, α	$\alpha_a+\alpha_c=2$	$\alpha_c=1$

liquid saturation. A linear function of saturation was employed by Berning and Djlali.[23] Here, we take the cubic relations for the relative permeabilities

$$k_{rl}=s^3 \quad \text{and} \quad k_{rg}=(1-s)^3 \qquad [9]$$

The presence of liquid phase affects the transport of species through the convection corrector factor, γ_c, and effective gas phase diffusivity, $D_g^{k,eff}$

$$\gamma_c=\begin{cases}\dfrac{\rho}{C^{H_2O}}\left(\dfrac{\lambda_l}{M^{H_2O}}+\dfrac{\lambda_g}{\rho_g}C_{sat}\right) & \text{for water}\\ \dfrac{\rho\lambda_g}{\rho_g(1-s)} & \text{for other species}\end{cases} \qquad [10]$$

where the relative mobilities of individual phases, λ_k, are

$$\lambda_l=\frac{k_{rl}/v_l}{k_{rl}/v_l+k_{rg}/v_g} \quad \text{and} \quad \lambda_g=1-\lambda_l \qquad [11]$$

The effective gas diffusion coefficient is given by

$$D_g^{k,eff}=[\epsilon(1-s)]^{1.5}D_g^k \qquad [12]$$

Note in Eq. 4 that in the isothermal model, the water vapor concentration in the two-phase zone is uniformly equal to the saturated value, thus the molecular diffusion of water vapor vanishes and the capillary-driven liquid water motion is responsible for water transport in the isothermal, two-phase zone. In the nonisothermal situation, the water/vapor saturation concentration, a strong function of temperature, however, varies and hence the vapor-phase diffusion emerges as a new transport mechanism along with the liquid water transport in the nonisothermal, two-phase zone.

In the presence of liquid water in the catalyst layer, the electrochemically active area is modified as follows

$$ai_0=(1-s)a_0i_0 \qquad [13]$$

Thermal transport.—Heat generation in the energy equation, Eq. 3, due to the electrochemical phenomena, can be summarized as follows[1,5,7]

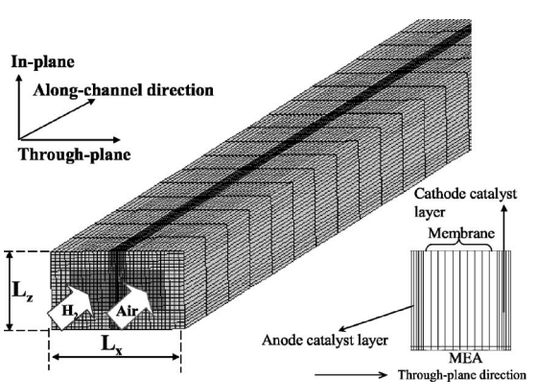

Figure 1. Computational domain and mesh of a single-channel PEFC.

In the catalyst layer $S_T=j\left(\eta+T\dfrac{dU_o}{dT}\right)+\dfrac{i_e^2}{\kappa^{eff}}+\dfrac{i_s^2}{\sigma^{eff}}$

In the membrane $S_T=\dfrac{i_e^2}{\kappa^{eff}}$

In the GDL and bipolar plate $S_T=\dfrac{i_s^2}{\sigma^{eff}}$ [14]

Here, $j\eta$ and $jT(dU_o/dT)$ are irreversible and entropic heats, respectively, generated from electrochemical reactions, which are dependent on local reaction current density, j, in the catalyst layer. i_e^2/κ^{eff} and i_s^2/κ^{eff} are Joule heating arising from protonic and electronic resistances, respectively, through the electrolyte and electronic phases. In addition, the heat release/absorption due to water condensation/evaporation is given by

$$S_T=h_{fg}\dot{m}_{fg} \qquad [15]$$

where h_{fg} and $\dot{m}_{fg}$ are the latent heat of vapor-liquid phase change and the phase change rate, respectively. The latter is readily calculated from the liquid continuity equation, namely[1,24]

$$\dot{m}_{fg}=\nabla\cdot(\rho_l\vec{u}_l) \qquad [16]$$

where the liquid-phase velocity in the M^2 model is computed from

$$\rho_l\vec{u}_l=\vec{j}_l+\lambda_l\rho\vec{u} \qquad [17]$$

Here $\vec{j}_l$ is the capillary diffusion flux calculated by

$$\vec{j}_l=\frac{\lambda_l\lambda_g}{\nu}K[\nabla P_c+(\rho_l-\rho_g)\vec{g}] \qquad [18]$$

The Leverett function is generally used to express the relationship between capillary pressure and liquid saturation in porous media, namely

$$P_c=P_l-P_g=\sigma\cos(\theta_c)\left(\frac{\epsilon}{K}\right)^{1/2}J(s) \qquad [19]$$

Here, σ is the surface tension and $J(s)$ is given by

$$J(s)=\begin{cases}1.417(1-s)-2.120(1-s)^2+1.263(1-s)^3 & \text{for } \theta_c<90^\circ\\ 1.417s-2.120s^2+1.263s^3 & \text{for } \theta_c>90^\circ\end{cases} \qquad [20]$$

The Leverett J-function only considers the influence of two characteristics of a porous medium, i.e., porosity and permeability, while ignoring the effect of detailed pore morphology.[32]

Finally, the advection term in the energy equation, Eq. 3, is modified by a correction factor, γ_T, given by

$$\gamma_T=\frac{\rho(\lambda_l c_{p,l}+\lambda_g c_{p,g})}{s\rho_l c_{p,l}+(1-s)\rho_g c_{p,g}} \qquad [21]$$

This correction is, however, inconsequential to the energy transport as the advection of both phases in GDL is negligible compared with

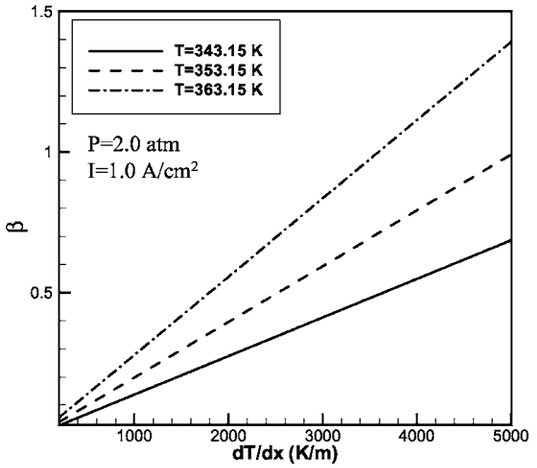

Figure 2. Functional dependence of β on temperature gradient.

heat conduction through the GDL matrix and the latent heat of condensation/evaporation.

Boundary conditions.[16,29,33]—Equations 1-6, form a complete set of governing equations with ten unknowns: $\vec{u}$ (three components), P, T, C^{H_2}, C^{O_2}, C^{H_2O}, ϕ_e, and ϕ_s. Their corresponding boundary conditions are described as follows:

Flow inlet boundaries.— The inlet velocity $\vec{u}_{in}$ in a gas channel is expressed by the respective stoichiometric flow ratio, i.e., ξ_a or ξ_c, defined at a reference current density, I_{ref} as

$$\xi_a = \frac{C^{H_2}\rho_a u_{in,a} A_a}{\frac{I_{ref}A}{2F}} \quad \text{and} \quad \xi_c = \frac{C^{O_2}\rho_c u_{in,c} A_c}{\frac{I_{ref}A}{4F}} \qquad [22]$$

where A_a and A_c are the flow cross-sectional areas of the anode and cathode gas channels, respectively. The inlet molar concentrations are determined by the inlet pressure, temperature, and humidity according to the ideal gas law.

Outlet boundaries.— Fully developed or no-flux conditions are applied

$$\frac{\partial \vec{u}}{\partial n} = 0, \quad \frac{\partial P}{\partial n} = 0, \quad \frac{\partial T}{\partial n} = 0, \quad \frac{\partial C_k}{\partial n} = 0, \quad \frac{\partial \phi_e}{\partial n} = 0, \quad \frac{\partial \phi_s}{\partial n} = 0 \qquad [23]$$

Walls.— No-slip and impermeable velocity condition and no-flux condition are applied

Table IV. Geometrical and operating parameters.[7,41]

Quantity	Value
Gas channel depth/ width	1.0/1.0 mm
Shoulder width	1.0 mm
GDL thickness, δ_{GDL}	0.2 mm
Catalyst layer thickness, δ_{CL}	0.01 mm
Membrane thickness, δ_m	0.018 mm
Fuel cell height/length	2.0/100.0 mm
Anode/cathode pressures, P	2.0/2.0 atm
Stoichiometry, ξ_a/ξ_c at 1.0 A/cm^2	2.0/2.0
Inlet temperature of gas flows, T_o	353.15 K
Relative humidity of anode/cathode inlet	100/100%
Porosity of GDLs, ϵ	0.6
Porosity of catalyst layers, ϵ_g	0.4
Volume fraction of ionomer in catalyst layers, ϵ_m	0.26
Thermal conductivity of membrane, k_{mem}^{eff}	0.95 W/m K
Thermal conductivity of catalyst layer, k_{CL}^{eff}	3.0 W/m K
Thermal conductivity of GDL, k_{GDL}^{eff}	3.0 W/m K
Thermal conductivity of bipolar plate, k_{land}^{eff}	20.0 W/m K
Viscosity of liquid water, μ_l	3.5×10^{-4} kg/m s
Surface tension, liquid-water-air (80°C), σ	0.0625 N/m
Contact angle, θ_c	110°
Permeability of GDL, K_{GDL}	10^{-12} m^2
Liquid-vapor phase change latent heat, h_{fg}	2.26×10^6 J/kg
Effective electronic conductivity in the GDL/Land, σ^{eff}	500/20000 S/m

$$\vec{u} = 0, \quad \frac{\partial C_k}{\partial n} = 0, \quad \frac{\partial P}{\partial n} = 0, \quad \frac{\partial \phi_e}{\partial n} = 0 \qquad [24]$$

In addition, the boundary conditions for the electronic phase potential, ϕ_s, and temperature, T, at the bipolar plate outer surfaces can be expressed as

$$\begin{cases} \phi_s = 0, & T = T_o & \text{Anode bipolar plate} \\ \phi_s = V_{cell}, & T = T_o & \text{Cathode bipolar plate} \\ \dfrac{\partial \phi_s}{\partial n} = 0, & \dfrac{\partial T}{\partial n} = 0 & \text{Otherwise} \end{cases} \qquad [25]$$

Numerical procedures.— The governing equations, Eq. 1-6, along with their appropriate boundary conditions, are discretized by the finite volume method[34] and solved in the commercial CFD software package, Fluent (version 6.0.12), by the SIMPLE (semi-implicit pressure linked equation) algorithm.[34] The SIMPLE algorithm updates the pressure and velocity fields from the solution of a pressure correction equation, solved by the algebraic multigrid (AMG) method. Following the solution of the flow field, species,

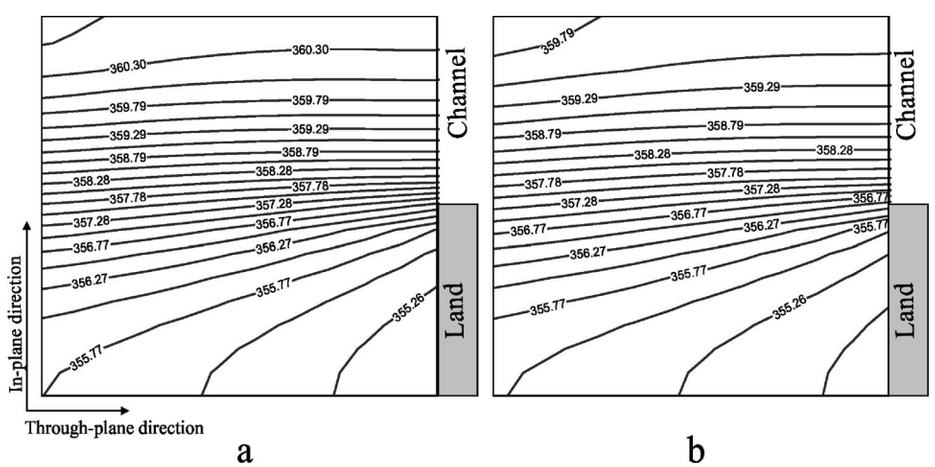

Figure 3. Temperature distributions in the cross-section of the cathode GDL in the inlet region for (a) case 1 and (b) case 2.

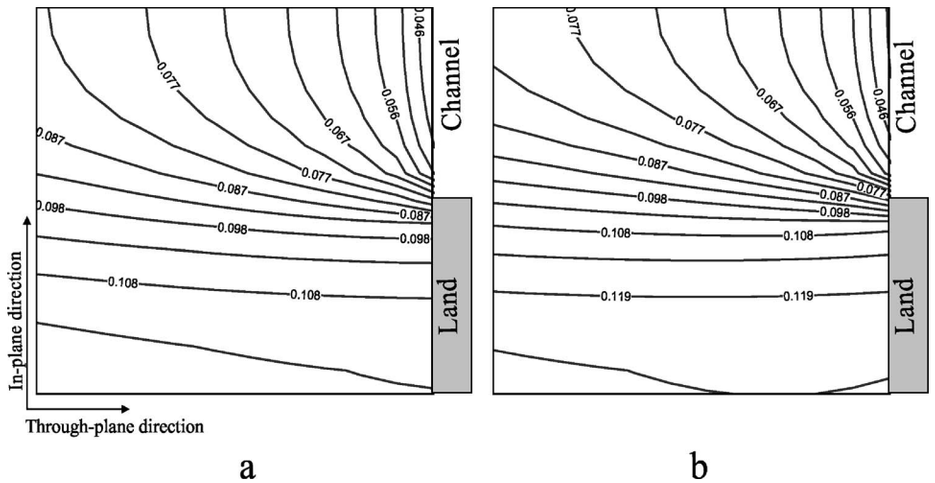

Figure 4. Liquid water saturation distributions in the cross-section of the cathode GDL in the inlet region for (a) case 1 and (b) case 2.

proton, and electron equations are solved. The source terms and physical properties are implemented in a UDF (user-defined function) and the species and charge transport equations are solved through the software's user-defined scalars.[35] The mesh of a single-channel PEFC employed here for a numerical study is shown in Fig. 1, with the anode and cathode in co-flow. Geometrical and operating parameters of this PEFC are listed in Table IV. A total of 120000 ($60 \times 100 \times 20$) computational cells are used to capture the complex electrochemical and physical phenomena in the PEFC. In addition, overall species balance is checked in addition to the equation residuals as important convergence criteria. These species balance checks also ensure physically meaningful results. In all the simulations to be presented in the next section, values of species imbalance (i.e., H_2, O_2, and H_2O) are all less than 1% and equation residuals are smaller than 10^{-6}.

Results and Discussion

Theoretical analysis.— Before presenting 3D numerical results, it is instructive to estimate the rate of vapor-phase diffusion in the nonisothermal, two-phase zone, as driven by the temperature gradient. To do so, we first estimate the temperature gradient within the GDL by assuming that the total heat released from the cell is removed mainly by lateral heat conduction between the catalyst layer and land.[7] It follows that

$$\frac{\Delta T}{\Delta x} \sim \frac{I(U_o - V)}{k^{\text{eff}}} \qquad [26]$$

where the total heat generation has been approximated by $I(U_o - V)$ with U_o being the thermodynamic equilibrium cell potential. Considering the current density of 1 A/cm^2 at 0.6 V and k^{eff} of 3.0 W/m K, one obtains the temperature gradient, $\Delta T/\Delta x$, equal to 2000 K/m.

In the two-phase zone, the rate of vapor-phase diffusion can be expressed as

$$D_{\text{g}}^{w,\text{eff}}(T,P)\frac{dC^w}{dx} = D_{\text{g}}^{w,\text{eff}}(T,P)\frac{dC_{\text{sat}}(T)}{dx} = D_{\text{g}}^{w,\text{eff}}(T,P)\frac{dC_{\text{sat}}}{dT}\frac{dT}{dx} \qquad [27]$$

To further determine the magnitude of the above term, we define a dimensionless factor, β, as the ratio of the vapor-phase diffusion flux to the water production rate in the cell, namely

$$\beta = \frac{D_{\text{g}}^{w,\text{eff}}(T,P)\dfrac{dC_{\text{sat}}(T)}{dT}}{\dfrac{I}{2F}}\frac{dT}{dx} \qquad [28]$$

The expressions of $C_{\text{sat}}(T)$ and $D_{\text{g}}^{w,\text{eff}}$ are listed in Table I. The graphs of β versus dT/dx are plotted in Fig. 2 for three different operating temperatures. It can be seen that β varies strongly with the operating temperature, T, and is equal to approximately 0.4 for $T = 80°C$ with a temperature gradient of 2000 K/m. This simple analysis implies that the vapor-phase diffusion removes ~40% of product water from the catalyst layer and hence its significance cannot be overlooked.

The vapor-phase diffusion through the nonisothermal, two-phase zone brings about phase change heat transfer between the catalyst layer and land. This is realized by water evaporation at the hotter catalyst layer, water vapor diffusion through the interstitial spaces of GDL, and subsequent vapor condensation on the cooler land surface. This mode of phase change heat transfer is conventionally referred to as the heat pipe effect. The amount of heat transported via this heat pipe effect can be estimated as follows

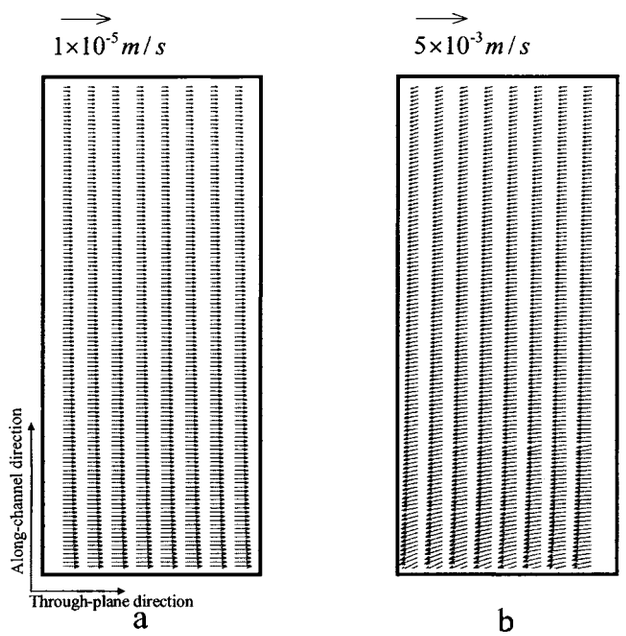

Figure 5. Velocity vectors in the cathode GDL at the middle section in case 2 for (a) liquid and (b) gas.

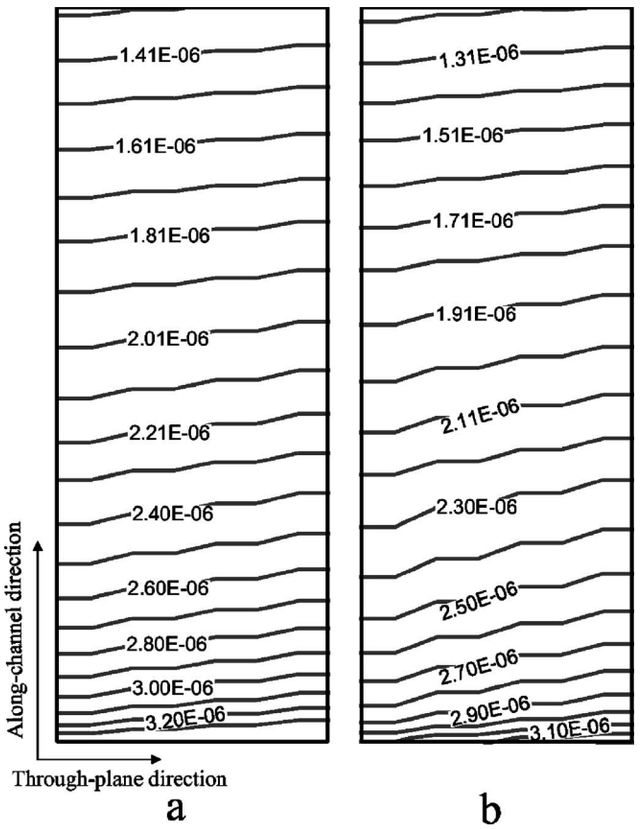

Figure 6. Contours of the liquid velocity component in the through-plane direction for (a) case 1 and (b) case 2.

$$h_{fg}\dot{m}_{fg} = h_{fg}M_w D_g^{w,eff}(T,P)\frac{dC_{sat}(T)}{dT}\frac{dT}{dx} = k_{fg}(T,P)\frac{dT}{dx} \quad [29]$$

It can be seen that the heat pipe effect can be described by an apparent thermal conductivity, $k_{fg}(T,P)$. Using the information contained in Fig. 2, k_{fg} is estimated to be ~0.42 W/m K at 80°C and becomes 0.56 W/m K at 90°C. The heat pipe effect thus amounts to 15–18% of heat conduction through the GDL matrix with a conductivity of 3 W/m K.

Numerical results.— To elucidate the intimate interplays between the two-phase transport and heat transfer, two cases have been simulated and contrasted for a single-channel PEFC. Case 1 ignores the vapor-phase diffusion in the two-phase zone as driven by the temperature gradient, while case 2 includes this effect and hence represents a full description of the two-phase, nonisothermal model. The average current density at 0.61 V is predicted to be 1.33 and 1.35 A/cm^2 for cases 1 and 2, respectively.

Figure 3 displays the temperature distributions in the cathode GDL for the two cases in the inlet region. We intentionally chose this upstream location as the local conditions in the gas channels are comparable between the two cases. It can be seen that the temperature varies by about 0.2 and 0.5 K across the GDL thickness under the channel and land, respectively, while it changes by ~5 K in the in-plane from the channel area to the land. Consequently, the actual temperature gradients, dT/dx, are around 1000 K/m (or $\beta \approx 0.2$) and 2500 K/m ($\beta \approx 0.5$) in the through-plane direction under the channel and land, respectively, and it is 5000 K/m ($\beta \approx 1.0$) in the in-plane direction, considering the geometrical sizes listed in Table IV. Thus, the water transport by vapor-phase diffusion occurs mostly in the in-plane direction from the channel area to the land. In addition, heat transfer between the catalyst layer and land is enhanced by the heat pipe effect as expressed by Eq. 29, thus decreasing the temperature level in case 2.

Figure 4 presents the liquid saturation distribution in the cathode GDL at the same inlet location. In the in-plane direction between the channel and land, the vapor-phase diffusion induced by the temperature gradient in GDL is directed from the channel area to the land, and thus opposes the capillary-driven liquid water transport from the land to the channel area. The net result of the opposed water transport mechanisms is that the liquid saturation becomes higher under the land when vapor transport under a thermal gradient is considered (i.e., case 2). The enlarged disparity in liquid saturation between the land and channel areas drives the additional liquid water rate to offset the vapor-phase diffusion of water along the opposite direction.

Figure 5 shows the liquid and gas velocity vectors in the GDL for case 2. It can be seen in Fig. 5a that the liquid velocity induced by capillary forces is on the order of 10^{-6} m/s, and decreases along the flow channel. In addition, this capillary-driven liquid flow is almost uniformly directed toward the channel, signifying the water removal by this capillary mechanism. The gas velocity, as shown in Fig. 5b, is on the magnitude of 10^{-3} m/s, and is uniformly in the direction of entering the GDL. The opposing gas and liquid water velocities have been also observed in Ref. 23. If we define the Peclet

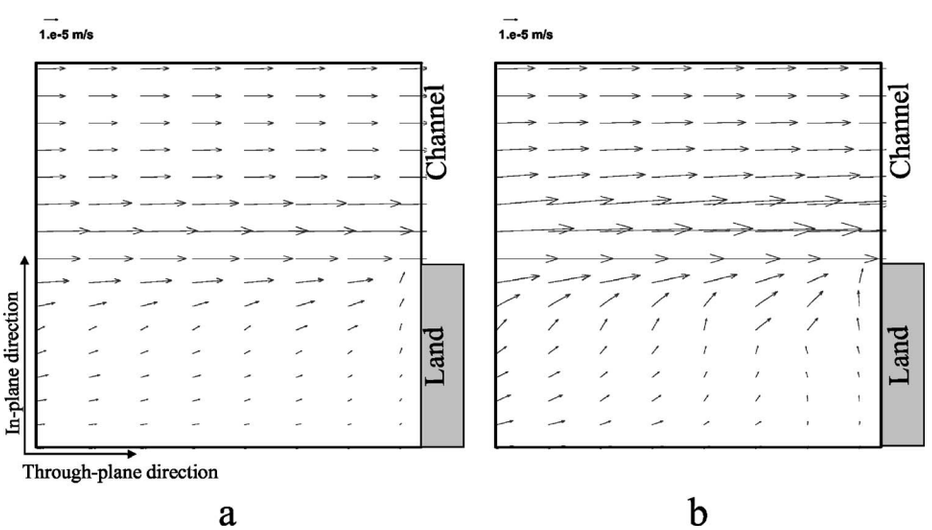

Figure 7. Liquid velocities in the cross-section of the cathode GDL in the inlet region for (a) case 1 and (b) case 2.

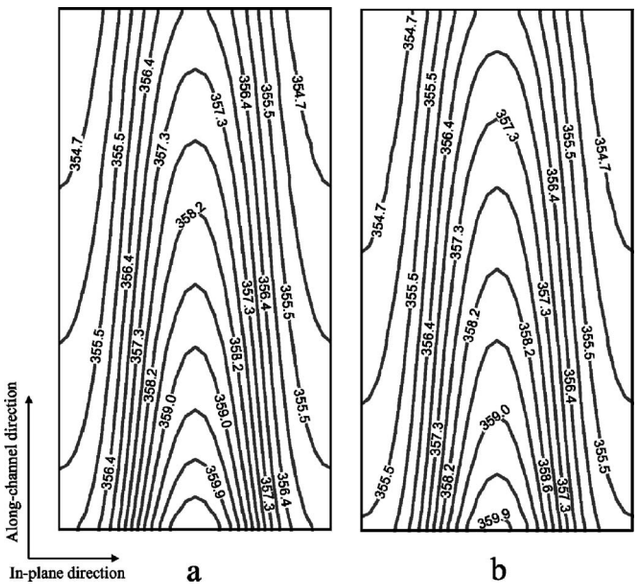

Figure 8. Contours of temperature in the membrane for (a) case 1 and (b) case 2.

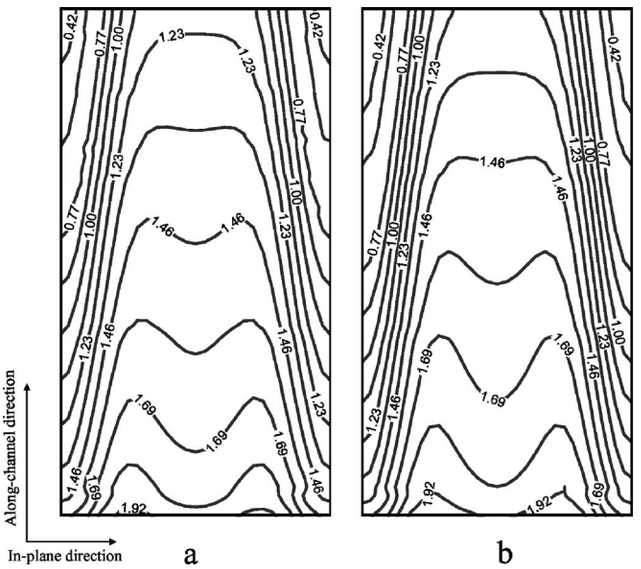

Figure 10. Current distributions for (a) case 1 and (b) case 2.

number as a parameter to measure the relative strength of this transverse gas convection to molecular diffusion, it follows that

$$\mathrm{Pe} = \frac{u\delta_{\mathrm{GDL}}}{D} \approx 0.1 \qquad [30]$$

This indicates that the convection effect in the gas phase is small compared to the diffusive transport.

Figure 6 compares the components of liquid velocity in the through-plane direction at the same location as Fig. 5 for the two cases. It can be seen that the liquid water flux due to capillary forces is slightly smaller in case 2, as shown in Fig. 6b, due to the fact that water removal through the GDL under the channel is enhanced by vapor-phase diffusion.

Figure 7 depicts the liquid velocity fields in the cross-section of the cathode GDL in the inlet region for the two cases. Focusing on the area under the land, it can be seen that liquid water flows away from the catalyst layer and bypasses the land to enter the channel area in both cases. However, for case 2, which considers vapor-phase diffusion and vapor condensation on the land surface, there is a stronger flow of liquid water from the land portion to the channel portion, especially in the areas close to the land surface.

Figure 8 compares the temperature distributions in the membrane for the two cases. It can be seen that case 2 features a slightly smaller temperature rise under the channel, again explained by the heat pipe effect as discussed in Fig. 3. In addition, the maximum temperature rise of $\sim$7 K appears under the channel, as expected, because the primary heat removal mechanism in PEFCs is via lateral heat conduction through GDL to the cooler land, whereas the gas convection to the gas stream plays a minor role.

Figure 9 presents the contours of liquid saturation at the CL/GDL interface on the cathode side for the two cases. It can be seen that the liquid saturation under the land is slightly higher in case 2 because of the vapor-phase diffusion that moves water vapor from the channel area to the land for condensation.

As mentioned earlier, the average current density of case 2 is 1.35 A/cm^2 versus 1.33 A/cm^2 of case 1. A comparison of the current distribution between the two cases is shown in Fig. 10. It can be seen that the local performance of case 2 under the channel is slightly improved due to water removal enhanced by vapor-phase diffusion, while it is slightly worse under the land due to the higher liquid saturation resulting from the vapor-phase diffusion and local condensation in the land area. In addition, the slightly lower temperature rise shown in Fig. 8 helps the cell performance in case 2 by alleviating dryness in the anode caused by water electro-osmotic drag.

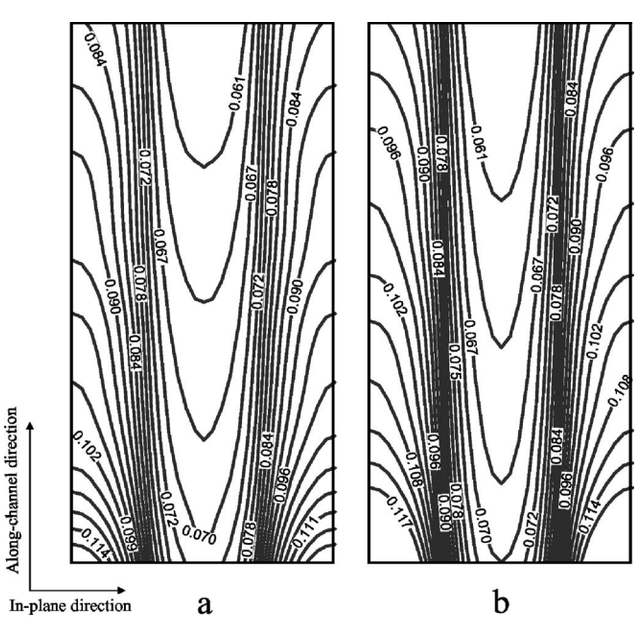

Figure 9. Contours of liquid saturation at the CL/GDL interface on the cathode side for (a) case 1 and (b) case 2.

Conclusions

A nonisothermal, two-phase model of polymer electrolyte fuel cells (PEFCs) has been developed to elucidate the interactions between two-phase transport and phase-change heat transfer. A theoretical analysis was performed to estimate the importance of vapor-phase diffusion driven by the temperature gradient in the two-phase zone and heat release/absorption due to phase change. It is found that the vapor-phase diffusion is capable of providing a flux compa-

rable to the water production rate from a PEFC and the consequent evaporation/condensation could transfer up to 15–18% of total heat generation. Three-dimensional simulations were carried out for a single-channel PEFC to compare two cases, one including the vapor-phase diffusion and the other ignoring it. It is found that vapor-phase diffusion transports water in the GDL from the channel area to the land area, causing more severe GDL flooding in the land portion. In the GDL underneath the channel, the vapor-phase diffusion enhances water removal to the gas channel. In addition, vapor-phase diffusion through the interstitial spaces of the GDL helps thermal dissipation via the heat pipe effect.

Acknowledgments

Support for this work by ECEC industrial sponsors is gratefully acknowledged.

The Pennsylvania State University assisted in meeting the publication costs of this article.

List of Symbols

A	electrode area, m^2
a	water activity; effective catalyst area per unit volume, m^2/m^3
a_o	catalyst surface area per unit volume, m^2/m^3
C_k	molar concentration of species k, mol/m^3
c_p	Specific heat, J/kg K
D	species diffusivity, m^2/s
EW	equivalent weight of dry membrane, kg/mol
F	Faraday's constant, 96487 C/equivalent
I	current density, A/cm^2
i	superficial current density, A/cm^2
j	transfer current density, A/cm^3
$\vec{j}_l$	mass flux of liquid phase, kg/m^2s
K	permeability, m^2
k	thermal conductivity, W/m K
k_r	relative permeability
L	length, m
M	molecular weight, kg/mol
mf_l^k	mass fraction of species k in liquid phase
n	the direction normal to the surface
n_d	electro-osmotic coefficient, H_2O/H^+
P	pressure, Pa
Pe	Peclet number
R	gas constant, 8.134 J/mol K
S	source term
s	stoichiometry coefficient in electrochemical reaction or liquid saturation
t	time, s
T	temperature, K
U_o	equilibrium potential, V
$\vec{u}$	velocity vector, m/s
V_{cell}	cell potential, V
X	mole fraction

Greek

α	transfer coefficient; net water flux per proton flux
ρ	density, kg/m^3
μ	viscosity, kg/m s
ν	kinematic viscosity, m^2/s
θ_c	contact angle, °
ϕ	phase potential, V
κ	proton conductivity, S/m
ξ	stoichiometric flow ratio
λ	membrane water content
λ_k	mobility of phase k
ε	porosity
η	surface overpotential, V
τ	shear stress, N/m^2
γ_c	correction factor for species convection
γ_T	correction factor for thermal convection
δ	thickness, m
σ	electronic conductivity, S/m; or surface tension, N/m

Superscripts and Subscripts

a	anode
c	cathode; capillary
CL	catalyst layer
e	electrolyte
eff	effective value
fg	phase change
g	gas phase
GDL	gas diffusion layer
in	inlet
k	species; liquid or gas phase
l	liquid
m	membrane phase
o	gas channel inlet value; reference value
ref	reference value
s	solid
sat	saturation value
w	water

References

1. C. Y. Wang, *Chem. Rev. (Washington, D.C.)*, **104**, 4727 (2004).
2. D. P. Wilkison and J. St-Pierre, Durability, in *Handbook of Fuel Cells: Fundamentals, Technology and Applications*, W. Vielstich, H. Gasteiger, and A. Lamm, Editors, Vol. 3, John Wiley & Sons, Ltd., New York (2003).
3. X. G. Yang, F. Y. Zhang, A. Lubawy, and C. Y. Wang, *Electrochem. Solid-State Lett.*, **7**, A408 (2004).
4. G. Maggio, V. Recupero, and C. Mantegazza, *J. Power Sources*, **62**, 167 (1996).
5. S. Mazumder and J. V. Cole, *J. Electrochem. Soc.*, **150**, A1503 (2003).
6. T. F. Fuller and J. Newman, *J. Electrochem. Soc.*, **140**, 1218 (1993).
7. H. Ju, H. Meng, and C. Y. Wang, *Int. J. Heat Mass Transfer*, **48**, 1303 (2005).
8. Z. H. Wang, C. Y. Wang, and K. S. Chen, *J. Power Sources*, **94**, 40 (2001).
9. D. Natarajan and T. V. Nguyen, *J. Electrochem. Soc.*, **148**, A1324 (2001).
10. A. Z. Weber, R. M. Darling, and J. Newman, *J. Electrochem. Soc.*, **151**, A1715 (2004).
11. L. You and H. Liu, *Int. J. Heat Mass Transfer*, **45**, 2277 (2002).
12. U. Pasaogullari and C. Y. Wang, *J. Electrochem. Soc.*, **151**, A399 (2004).
13. U. Pasaogullari and C. Y. Wang, *Electrochim. Acta*, **49**, 4359 (2004).
14. C. Ziegler, H. M. Yu, and J. O. Schumacher, *J. Electrochem. Soc.*, **152**, A1555 (2005).
15. H. Sun, H. Liu, and L.-J. Guo, *J. Power Sources*, **143**, 125 (2005).
16. U. Pasaogullari and C. Y. Wang, *J. Electrochem. Soc.*, **152**, A380 (2005).
17. H. Meng and C. Y. Wang, *J. Electrochem. Soc.*, **152**, A1733 (2005).
18. G. Lin and T. Van Nguyen, *J. Electrochem. Soc.*, **153**, A372 (2006).
19. J.-H. Nam and M. Kaviany, *Int. J. Heat Mass Transfer*, **46**, 4595 (2003).
20. A. Rowe and X. Li, *J. Power Sources*, **102**, 82 (2001).
21. J. Yuan and B. Sunden, *Electrochim. Acta*, **50**, 677 (2004).
22. P. Costamagna, *Chem. Eng. Sci.*, **56**, 323 (2001).
23. T. Berning and N. Djilali, *J. Electrochem. Soc.*, **150**, A1589 (2003).
24. C. Y. Wang and P. Cheng, *Adv. Heat Transfer*, **30**, 93 (1997).
25. S. Shimpalee and S. Dutta, *Numer. Heat Transfer, Part A*, **38**, 111 (2000).
26. S. Dutta, S. Shimpalee, and J. W. Van Zee, *J. Appl. Electrochem.*, **30**, 135 (2000).
27. S. Mazumder and J. V. Cole, *J. Electrochem. Soc.*, **150**, 1510 (2003).
28. E. Birgersson, M. Noponen, and M. Vynnycky, *J. Electrochem. Soc.*, **152**, A1021 (2005).
29. H. Meng and C. Y. Wang, *J. Electrochem. Soc.*, **151**, A358 (2004).
30. Y. Wang and C. Y. Wang, *J. Power Sources*, **153**, 130 (2006).
31. Y. Wang and C. Y. Wang, *J. Electrochem. Soc.*, **152**, A445 (2005).
32. F. A. L. Dullien, *Porous Media: Fluid Transport and Pore Structure*, Academic Press, San Diego (1992).
33. Y. Wang and C. Y. Wang, *J. Power Sources*, **147**, 148 (2005).
34. S. V. Patankar, *Numerical Heat Transfer and Fluid Flow*, Hemisphere Publishing Corp., New York (1980).
35. Fluent 6.1 UDF Manual, Fluent Inc. (2003).
36. T. E. Springer, T. A. Zawodinski, and S. Gottesfeld, *J. Electrochem. Soc.*, **126**, 2334 (1991).
37. S. Motupally, A. J. Becker, and J. W. Weidner, *J. Electrochem. Soc.*, **147**, 3171 (2000).
38. T. A. Zawodzinski, J. Davey, J. Valerio, and S. Gottesfeld, *Electrochim. Acta*, **40**, 297 (1995).
39. A. C. West and T. F. Fuller, *J. Appl. Electrochem.*, **26**, 557 (1996).
40. R. B. Bird, W. E. Stewart, and E. N. Lightfoot, *Transport Phenomena*, John Wiley & Sons, New York (1960).
41. Y. Wang and C. Y. Wang, *Electrochim. Acta*, **50**, 1307 (2005).
42. F. P. Incropera and D. P. DeWitt, *Fundamentals of Heat and Mass Transfer*, John Wiley & Sons, New York (1996).